Front. Phys.
DOI 10.1007/s11467-013-0305-0

REVIEW ARTICLE

Semiconductor nanowires for photovoltaic and photoelectrochemical energy conversion

Neil P. Dasgupta[1], **Peidong Yang**[1,2,†]

[1] *Department of Chemistry, University of California, Berkeley, CA 94720, USA*
[2] *The Center of Excellence for Advanced Materials Research (CEAMR), Chemistry Department, King Abdulaziz University, Jeddah 21589, Saudi Arabia*
E-mail: [†] *p_yang@uclink.berkeley.edu*
Received January 18, 2013; accepted February 12, 2013

Semiconductor nanowires (NW) possess several beneficial properties for efficient conversion of solar energy into electricity and chemical energy. Due to their efficient absorption of light, short distances for minority carriers to travel, high surface-to-volume ratios, and the availability of scalable synthesis methods, they provide a pathway to address the low cost-to-power requirements for widescale adaptation of solar energy conversion technologies. Here we highlight recent progress in our group towards implementation of NW components as photovoltaic and photoelectrochemical energy conversion devices. An emphasis is placed on the unique properties of these one-dimensional (1D) structures, which enable the use of abundant, low-cost materials and improved energy conversion efficiency compared to bulk devices.

Keywords nanowire, photovoltaics, artificial photosynthesis, photoelectrochemistry, solar energy

PACS numbers 62.23.Hj, 63.22.Gh, 84.60.Lw, 84.60.-h

Contents

1 Introduction

The dramatic increase in energy supply requirements facing humanity in the 21st century, combined with the negative environmental impacts of fossil fuel combustion, have led to an urgent need for the large-scale deployment of renewable energy and energy efficiency technologies. Among the renewable sources of energy available on earth, the solar flux represents by far the largest source, with an average incident energy flux which is on the order of 10^4 times larger than the total global power consumption. However, implementation of solar energy technologies has been limited by high costs and resource intermittency issues. Accordingly, there has been an explosion in research on conversion and storage of solar energy, with an emphasis on increasing efficiency and decreasing manufacturing costs.

In order to efficiently convert solar energy to electricity or stored energy in chemical bonds, the solar resource must be effectively absorbed, and this absorbed energy must be extracted before losses due to heat dissipation occur. Fundamentally, this requires three processes to occur: absorption of a large portion of the electromagnetic radiation from the sun to generate excited charge carriers, diffusion of charge carriers to an interface, and separation of these excited charge carriers before recombination losses occur. Additionally, we must search for

materials and device architectures which can facilitate these processes without the need for expensive manufacturing techniques such as high vacuum or temperature levels, or the use of precious, non-earth-abundant materials. These systems must be scalable to the terawatt (TW) levels required for large-scale deployment of renewable energy on a global scale.

To address these challenges, nanostructured architectures have been explored due to a variety of advantages they possess compared to "bulk" materials. For example, the characteristic length scales of solar energy conversion, such as the wavelength of light and the diffusion length of excited carriers in a semiconductor, are typically on the nanometer to micrometer length scale. This allows for novel phenomena such as optical and electrical confinement, stabilization of metastable material phases, and geometric advantages such as high surface-to-volume ratios, all of which can dramatically affect the physics and chemistry of devices with components at these length scales. Furthermore, there have been significant advances in fabrication techniques for nanomaterials in the past several decades, improving the ability to reproducibly fabricate high-quality devices using robust and high-throughput manufacturing methods.

Among the various categories of nanomaterials, semiconductor nanowires (NWs) are of particular interest in solar energy conversion devices due to a combination of several favorable properties [1, 2]. NWs can benefit the absorption, diffusion, and charge separation steps of solar energy devices due to the unique properties of one-dimensional (1D) materials at these length scales. For example, by fabricating vertical NW arrays the absorption length (L_A) required to fully utilize the solar spectrum can be decoupled from the carrier extraction length (L_D), which should be minimized to reduce recombination [3], as shown in Fig. 1. Additionally, NW templates suppress reflection and enhance light scattering and trapping [4–8]. This permits the use of significantly less material than a planar architecture, and reduces the purity and morphological requirements of the absorber layer due to a decreased carrier extraction length. As a result, NW devices have the potential to lower the cost of solar devices both by decreasing the energy input required for material purification, and by enabling new material systems based on abundant, low-cost elements which are not generally effective in planar geometries due to incompatible absorption and diffusion length scales.

In this article, we will highlight recent advances by our group in the application of semiconductor NWs to photovoltaic (PV) and photoelectrochemical (PEC) energy conversion. This is not intended to be a comprehensive review of the field, but rather a set of examples which demonstrate the unique properties of these 1D materials.

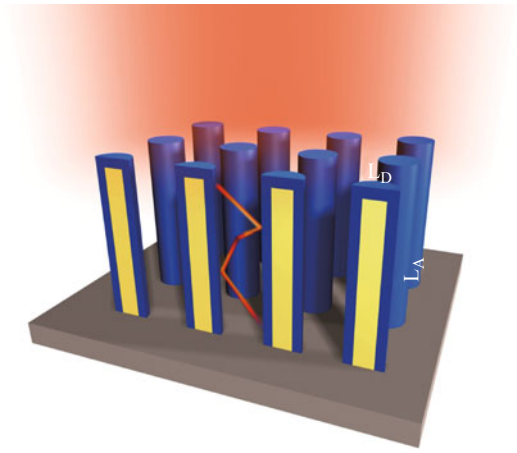

Fig. 1 Vertical NW photovoltaic device, with a radial p-n junction. This allows for the photon absorption length (L_A, associated with the NW length) to be decoupled from the carrier diffusion length (L_D associated with the NW radius), as well as efficient light scattering and trapping. This enables the use of abundant, low-cost materials with reduced purity requirements and lower raw material usage compared to bulk devices.

Our approach involves a combination of investigating single-NW devices to gain a fundamental understanding of the energy conversion and transport properties at the nanoscale with the development of larger-scale NW array devices for macroscopic energy conversion. An emphasis will be placed on the unique characteristics and benefits of using NWs for solar energy conversion, as well as the associated challenges and directions for future research.

2 Nanowire photovoltaics

PV cells convert light energy directly into electricity through excitation of electron-hole pairs in a semiconductor material, which are subsequently separated to external electrodes, providing a voltage and photocurrent available for producing useful work. The current PV market is dominated by crystalline Si cells, which are able to achieve efficiencies of around 25% [9], but are expensive to manufacture due to the high material costs. In order to decrease the material cost, the use of cheaper materials such as polycrystalline thin films or organic semiconductors is possible. Additionally, managing light in such a way that the solar resource is concentrated to a smaller area or trapped inside the absorber layer of the cell can decrease the amount of material required to fully absorb the light. To further reduce the cost requires new manufacturing techniques and architectures capable of minimizing loss mechanisms such as recombination, reflection and parasitic resistances, while using low-cost fabrication techniques and material systems. Due to the aforementioned advantages of NWs, our group has been exploring their implementation into vertical-array and

single-NW PV devices.

2.1 ZnO nanowire array PVs

Our initial efforts on NW PV array devices were based on ZnO NW arrays given their favorable optical, electronic, and geometric properties. This was facilitated by the development of low-temperature, solution-based processing of high quality single-crystalline ZnO NW arrays [10, 11]. These arrays exhibit favorable properties for PV energy conversion when combined with materials that suffer from poor diffusion lengths such as polymers or defective semiconductors. The solution-based processing allows for a scalable, low-cost fabrication on a variety of substrates, which could help drive down the costs of PV manufacturing.

To demonstrate the ability to fabricate functional PV devices using these ZnO NW arrays, a modified version of the dye-sensitized solar cell (DSSC) was developed, in which the mesoporous nanoparticle film used for dye loading was replaced with a vertical ZnO NW array, as shown in Fig. 2(a) [12]. This architecture presents several advantages compared to a nanoparticle film. While the transport of charge carriers in the nanoparticle films is dominated by trap-limited diffusion [13], the use of vertical single-crystalline NWs provides a direct pathway for charge extraction, leading to faster charge collection in the NW cell. Furthermore, the NW geometry allows for the formation of a full depletion layer at the semiconductor-electrolyte interface, leading to the formation of a radial electric field which assists charge separation. The complimentary electric fields in the radial and vertical directions assist charge separation and extraction respectively, and allow for improved charge transport compared to nanoparticle films. In addition, an increase in the charge injection rate was measured in the NW electrodes, due to a homogeneous crystallographic orientation along the NW surface.

The overall efficiency of the initial NW DSSCs was limited to 1.5%, primarily due to the lower surface area of the NW array compared to the nanoparticle film, which limits light absorption. In Fig. 2(b), a comparison of J_{sc} vs. roughness factor is shown between the ZnO NW electrodes, and nanoparticle films of TiO_2 and ZnO. The ZnO NW electrode shows similar behavior in the TiO_2 nanoparticle film despite being $\sim$10$\times$ longer in the thickness direction, and better performance than both of the ZnO nanoparticle films. This is direct evidence of an improved charge collection due to the NW geometry. A subsequent study demonstrated that the efficiency of the ZnO NW DSSCs could be further improved by coating the NW surface with a thin TiO_2 layer deposited by atomic layer deposition (ALD), which led to an increase in the V_{oc} and fill factor due to a decrease in recombination at the semiconductor/electrolyte interface [14]. Further improvements in the efficiency would be possible by increasing the NW surface area.

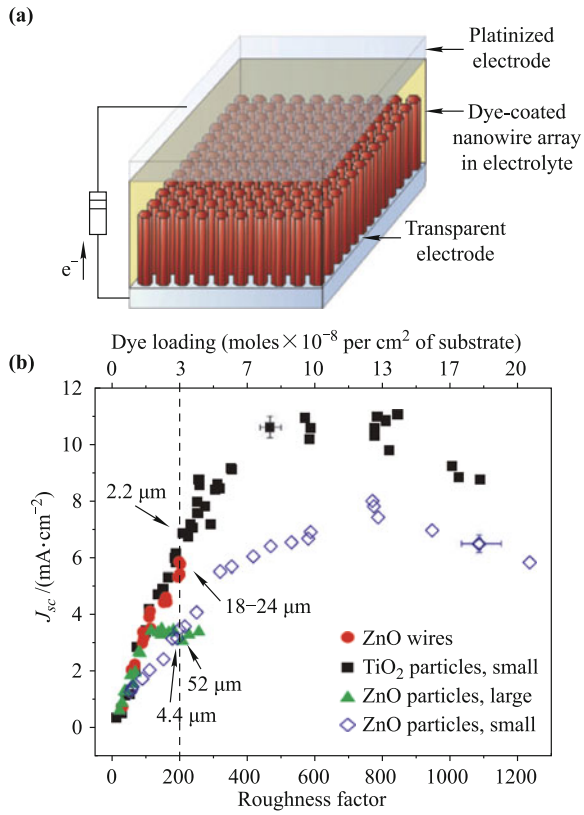

Fig. 2 **(a)** Schematic representation of a NW DSSC. **(b)** Comparison of J_{sc} vs. roughness factor between NW and nanoparticle electrodes. The ZnO NW electrode exhibits superior performance to ZnO nanoparticle electrodes, and exhibits similar performance to the TiO_2 electrode for roughness factors up to 200. Reproduced from Ref. [12], Copyright © 2005 Nature Publishing Group.

Beyond DSSCs, ZnO NW arrays have been explored for other material systems with short minority carrier diffusion lengths in the absorbing layer. For example, inorganic-organic hybrid NWs have been studied as a replacement for bulk heterojunction cells, due to improved charge transport in the inorganic electrode with a direct current path, similar to the DSSC. It was shown that an ALD TiO_2 coating on hydrothermal ZnO NW arrays leads to an improvement in performance in ZnO-P3HT cells, due to an improvement in fill factor and V_{oc} [15]. This phenomenon was also demonstrated in all-oxide NW PV devices, consisting of ZnO NWs in contact with a p-type Cu_2O phase [16]. While the overall efficiencies of these devices remains below 1%, these studies demonstrated the importance of several critical factors, including the ability to form a high-quality interface with low recombination rates to achieve improved performance in NW PV devices, while minimizing undesirable losses due to shunting. If improved interfacial proper-

ties can be achieved, these architectures provide an ideal platform to extract charge carriers from low-cost materials which suffer from short minority carrier diffusion lengths.

2.2 Silicon nanowire array PVs

Due to the large elemental abundance and the vast amount of research and development of Si processing technology, it is likely that Si will maintain a significant portion of the PV market share in the near future. Planar single-crystalline Si cells are a mature technology, with only marginal room for improvements in efficiency. Therefore, reducing the $/watt module cost will require new ways to make inexpensive Si cells, while also maintaining high efficiencies.

To reduce the cost of Si PVs, our group has employed two strategies. The first is to utilize significantly less raw material, by improving the optical absorption of Si. Due to the relatively low absorption coefficient of Si in visible wavelengths compared to direct bandgap semiconductors, a thickness of several hundreds of microns is typically required to fully absorb the solar spectrum in single-crystalline Si PVs. One way to mitigate this requirement is to increase the effective path length of light in the material through optical scattering and light trapping strategies.

Several groups have investigated the anti-reflection properties of microwire [17], nanowire [4, 6–8] and tapered nanocone [18, 19] geometries, which leads to a reduction in the losses at the top surface of the PV cell. In addition to suppressing reflection, we have demonstrated that nanowire arrays are very efficient at light trapping, leading to an enhancement of the optical path length compared to a planar absorber [5]. This permits the use of significantly less material than a bulk crystalline PV by reducing both the overall density of material in the absorber layer, and the required thickness of the cell.

Light-trapping was investigated in top-down NW arrays fabricated by nanosphere lithography and anisotropic dry etching of crystalline Si substrates, as shown in Fig. 3(a) and (b). This permitted simple and accurate control of the NW diameter and length by controlling the size of the masking nanosphere and etching time respectively. Radial p–n junctions were fabricated by subsequent diffusion doping, and PV performance was tested as a function of NW length. Interestingly, when the NW length was increased from 8–20 μm, the short-circuit photocurrent (J_{sc}) only increased by 2%, compared to a 22% increase in planar control samples of the same thicknesses. This suggested a strong light-trapping effect in NW arrays, which was further investigated by transmission measurements.

To quantify the light-trapping capability of the Si NW arrays, free-standing Si-thin films on transparent SiO_2 support layers were fabricated by back-etching silicon on insulator (SOI) wafers, and transmission measurements were performed through the thin membranes. These thin Si films were subsequently patterned and etched to form NWs, and the optical transmission was observed to decrease across a broad range of visible and near-IR wavelengths, as shown in Fig. 3(c). As the length of the NWs increased, the transmission decreased, despite the fact that the etching process was actually removing a significant amount material from the absorber layer. By comparing the J_{sc} of thin PV devices with different NW lengths, an increase in the optical path length enhancement was observed with increasing NW length. An increase in the path length of up to 73 was observed, which exceeds the randomized scattering (Lambertian) limit ($2n^2 \sim 25$) without a back reflector [20]. This demonstrates the ability of NW architectures to reduce the raw material requirements to fully absorb the solar spectrum, which could eventually lead to decreased PV manufacturing costs as our ability to fabricate uniform NW arrays on low-cost substrates continues to improve.

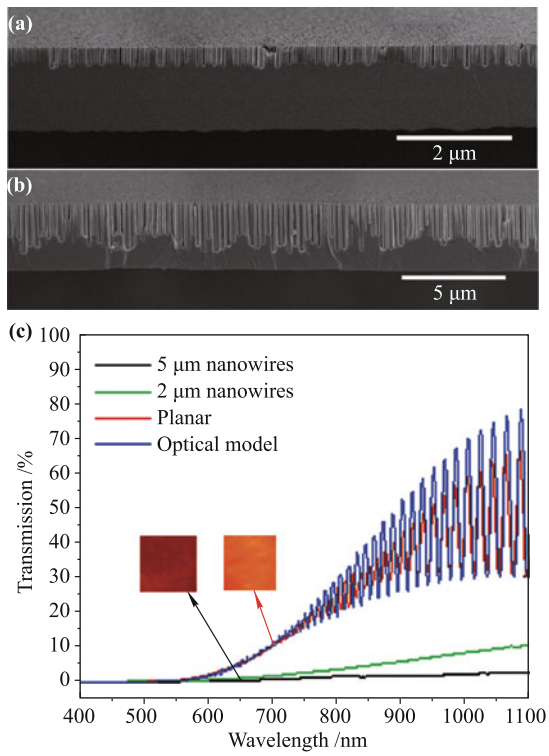

Fig. 3 Optical measurements of Silicon NW arrays of various lengths. Cross-sectional SEM image of Si NW arrays with lengths of **(a)** 2 μm and **(b)** 5 μm. **(c)** Transmission spectra of planar and NW samples. NW samples exhibit significantly decreased transmission across a broad wavelength range due to increased light-trapping in the NW arrays. Reproduced from Ref. [5], Copyright © 2010 American Chemical Society.

Besides reducing the volume of raw material required

to fully absorb the solar irradiation, another strategy to lower cost is to reduce the purity requirements of the semiconductor material. For example, the cost of metallurgical-grade Si is estimated to be on the order of 100 times lower than that of solar-grade Si [21]. However, impurities in a semiconductor can lead to recombination at defects, leading to a reduction in the minority carrier diffusion length. This leads to an inherent mismatch between the material thickness required to fully absorb the solar spectrum, and distance that excited carriers can diffuse before recombining. As shown in Fig. 1, radial p–n junctions in vertical NW arrays can mitigate this problem, by orthogonalizing the absorption dimension (associated with the NW length) and carrier extraction dimension (associated with the NW diameter) [3].

To demonstrate this effect, we studied the performance of Cu contaminated single-crystalline PVs [22]. To fabricate the devices, a thin film of Cu was sputtered on the surface of p-Si wafers, and a high-temperature anneal was performed to diffuse the Cu into the Si substrate. This was followed by a wet etch to remove the Cu residue remaining on the wafer surface. The Cu concentration in the wafer was measured by Secondary Ion Mass Spectrometry, and a concentration of up to 10^{20} cm^{-3} was observed near the surface, which plateaus above 10^{17} cm^{-3} after the first micron of depth profiling. Subsequently, nano- to micro-scale holes were etched to a depth of 6–10 μm into the wafer by deep reactive ion etching (DRIE). Radial p–n junctions were formed by spin-coating and diffusion annealing a phosphorous dopant, and finally, metal top contacts were deposited.

The PV performance of these Cu-contaminated materials was tested by fabricating planar devices, which were compared to Si devices without the impurities. A significant decrease in efficiency was observed in the "dirty" cells, due to the presence of the impurities. However, when the patterned radial p–n junction structure was fabricated in the contaminated cells, an improvement in the device efficiency was observed, with the greatest improvement measured for devices with a 4 μm pitch between the holes. The improvement in efficiency was due to a larger short-circuit current in the radial devices, which was attributed to improved collection efficiency of minority carriers in the contaminated cells due to a shorter diffusion length. For larger pitches, a smaller improvement in efficiency was observed. When the pitch was reduced to 500 nm, a dramatic reduction in efficiency was observed, to levels below the planar devices.

The dependence of efficiency on the periodicity of a radial p–n junction array can be understood by considering the competition between improvements due to a shorter minority carrier diffusion length, and the ability to fully deplete the semiconductor to form a p–n junction. As the pitch is decreased to values approaching L_{D}, the collection efficiency increases due to less recombination from carriers that cannot effectively diffuse to the junction. Once the pitch is equal to or less than L_{D}, a point of "diminishing returns" occurs, where the volume over which carriers are effectively collected begins to overlap, no longer providing an improvement in short-circuit current. At this point, efficiency is likely to decrease, due to an increase in surface recombination from a larger junction area. Eventually, when the pitch decreases below the depletion width of the p–n junction, an overlap in depletion regions occurs and the core-region is unable to achieve a fully depleted diode, reducing the maximum available V_{oc} and efficiency.

These examples demonstrate several of the benefits of NW PVs, including improved optical properties and reduced material volume and purity requirements. Additionally, several challenges associated with balancing efficient charge extraction, while minimizing surface recombination, have been identified. Further optimization of NW PV structures will require a fundamental and quantitative understanding of the effects of geometric and material properties, and an improved control of the interfaces. Accordingly, we have focused significant efforts on studying single-NW PV devices, which allow for a careful study of the impact of these variables at the nanoscale, while removing variables associated with naturally occurring variations in large ensembles of NWs in an array and parasitic losses such as shunting pathways resulting from macroscopic processing.

2.3 Single-nanowire PVs

Single-NW PV devices allow for an improved quantitative analysis of performance by reducing variations associated feature size, interfacial quality, and other nonuniformities in large-scale arrays [23–25]. For example, in polymer-inorganic hybrid PVs, an improved understanding of the interfacial properties is crucial to increase device efficiencies [26], but can be difficult to analyze in large-scale devices due to localized variations in material properties and interface quality. To address this issue, we fabricated individual NW inorganic-organic hybrid PV devices consisting of a single-crystalline ZnO NW core and an organic shell of end-functionalized oligo- and polythiophenes, which were grafted onto the NW surface using solution processing techniques to form a radial p-n junction [27]. Individual NWs were characterized by TEM, showing a core-shell structure, allowing for a visualization of the morphology of the inorganic-organic interface. Planar single-NW devices were fabricated on an insulating substrate, and individual contacts were made to the core and shell regions. The J–V characteristics

showed higher V_{oc} values than array devices, suggesting that the quality of the grafted interface is higher than that formed by solution processing. On the other hand, the devices had lower J_{sc} values than theoretically predicted, illustrating the limitations of absorption and charge separation in these organic absorber materials. Despite the relatively low overall efficiencies of these devices, the single-NW PV platform proved to be an effective platform to study the various factors affecting device performance in macroscopic cells.

While NW-based devices have demonstrated various optical and charge separation benefits, they are still typically less efficient than planar devices of the same material system [24, 25, 28]. This is typically related to a lower V_{oc} and fill factor in the NW devices due to increased interfacial recombination from the large junction surface area. This is particularly evident in the inorganic-polymer hybrid devices. To address this issue, we developed a simple method to produce high-quality epitaxial interfaces in radial p-n junctions by using mild solution processing [29]. A cation exchange reaction was used to form epitaxial CdS/Cu_2S core-shell NWs, which exhibited V_{oc} and fill factors of 0.6 V and 80% in a single NW device (Fig. 4). These values are larger than equivalent planar devices, with a lower drop in V_{oc} in the NW devices with reduced light intensity. This is attributed to the high-quality interface in this single-crystalline core-shell structure, leading to improved collection efficiency. An overall efficiency of 5.6% was measured, which was limited only by a lower J_{sc} than the theoretical maximum, due to insufficient absorption of visible wavelengths in the thin Cu_2S shell. This suggests that increasing the shell thickness, while maintaining the benefits of the high-quality interface would lead to even higher efficiencies.

An additional benefit of fabricating horizontal devices is the ability to study the uniformity of charge collection as a function of position in and individual NW. To accomplish this, scanning photocurrent mapping (SPCM) was performed, demonstrating that the core-shell region was active for charge separation, with a sharp drop-off at the edge of this region. This illustrates the importance of a radial p-n junction in this system, which benefits collection of charge from the CdS material which suffers from a low minority carrier diffusion length (<1 μm). Furthermore, multiple devices could be fabricated from a single NW, allowing for series and parallel configurations which are current or voltage matched due to the use of the same NW. This demonstration of an improved performance in a NW PV device compared to planar equivalents using simple, and potentially low-cost processing, is an important indication of the potential benefits of core-shell NWs in solar cells.

Beyond studying the importance of the radial p-n interface quality on device performance, single-NW devices can be used to quantify the optical benefits associated with subwavelength interactions between light and the nanostructure. For example, individual NWs have been shown to support leaky-mode resonances, which can enhance light absorption at resonant wavelengths [30, 31]. Additionally, metal nanoparticles are being actively studied as a way to enhance absorption in PV materials through plasmonic manipulation of light [32–34]. Both of these phenomena involve interaction of light with

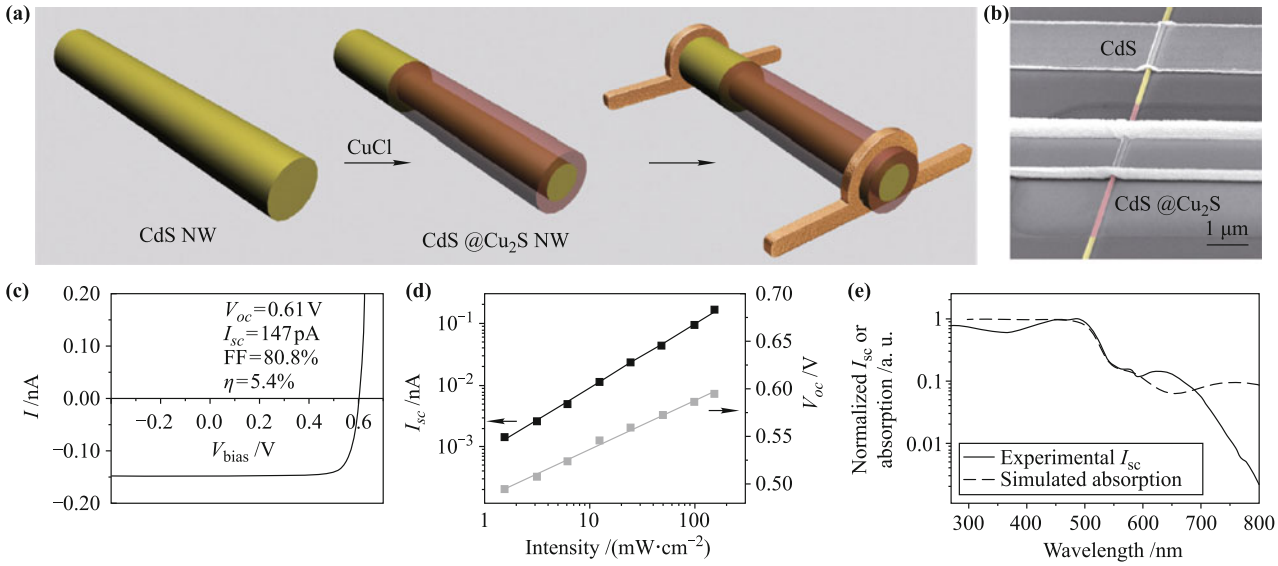

Fig. 4 Core-shell CdS/Cu_2S single-NW PVs. **(a)** Schematic of the fabrication process. A core-shell structure is formed by solution-based cation exchange of the CdS NW in a solution containing Cu ions. to form a Cu_2S shell. **(b)** SEM image of a single-NW PV device. **(c)** *I–V* curve of a single-NW PV device under 1 sun (AM 1.5 G) irradiation. **(d)** Variation of I_{sc} and V_{oc} on light-intensity **(e)** Wavelength-dependence of photocurrent compared with simulated absorption. Reproduced from Ref. [29], Copyright © 2011 Nature Publishing Group.

subwavelength features, which could potentially increase the performance of PV devices.

To study these effects, we fabricated a single-NW Si PV device decorated with an octahedral silver nanocrystal [35]. Si NWs were grown in a bridging configuration between two electrodes, using VLS growth in a CVD reaction. Radial p-n junctions were fabricated using a series of lithography and masking steps followed by vapor-phase doping. To study the absorption properties of these NWs, wavelength-dependent photocurrent measurements were taken on the devices. These measurements show that the NW devices exhibit peaks in photocurrent associated with optical resonances of the wire, which were in agreement with numerical simulations of the absorption using a three-dimensional finite-difference time domain (FDTD) method.

When a single silver nanocrystal was deposited onto a single-NW PV device, changes in the wavelength-dependent photocurrent were observed. The experimental results showed an increase in photocurrent at wavelengths associated with plasmon resonances in the nanoparticle, and a decrease at wavelengths associated with the optical resonances of the NW (Fig. 5). These effects are in agreement with FDTD simulations of the NW-nanocrystal system, which predict a perturbation of the NW resonances by the nanoparticle. This study demonstrates the power of single-NW PV devices to quantitatively study the optical properties of nanostructured geometries, providing insight into the design of future devices which could benefit from enhanced absorption from these subwavelength effects.

Our research in NW PV devices has demonstrated many benefits of these structures associated with improved light absorption and charge separation in radial p-n junctions. The importance of a high-quality interface has been demonstrated, and a quantitative analysis of individual interfaces has been achieved by use of single-NW devices. The importance of balancing these benefits with potential disadvantages associated with increased surface/interface recombination remains a critical engineering challenge, which requires further insights into the effects of geometric and material variables on device performance. Nevertheless, significant progress has been made towards the development of efficient NW PVs, which could dramatically reduce the cost of PV technology by decreasing material loading and purity requirements, while maintaining high efficiencies. In the next section, we will discuss how many of these same benefits can be utilized to design photoelectrochemical (PEC) cells, which store solar energy in the form of chemical bonds, which can later be utilized as a renewable fuel source.

3 Nanowires for photoelectrochemical energy conversion

Due to the intermittency of the solar resource, energy

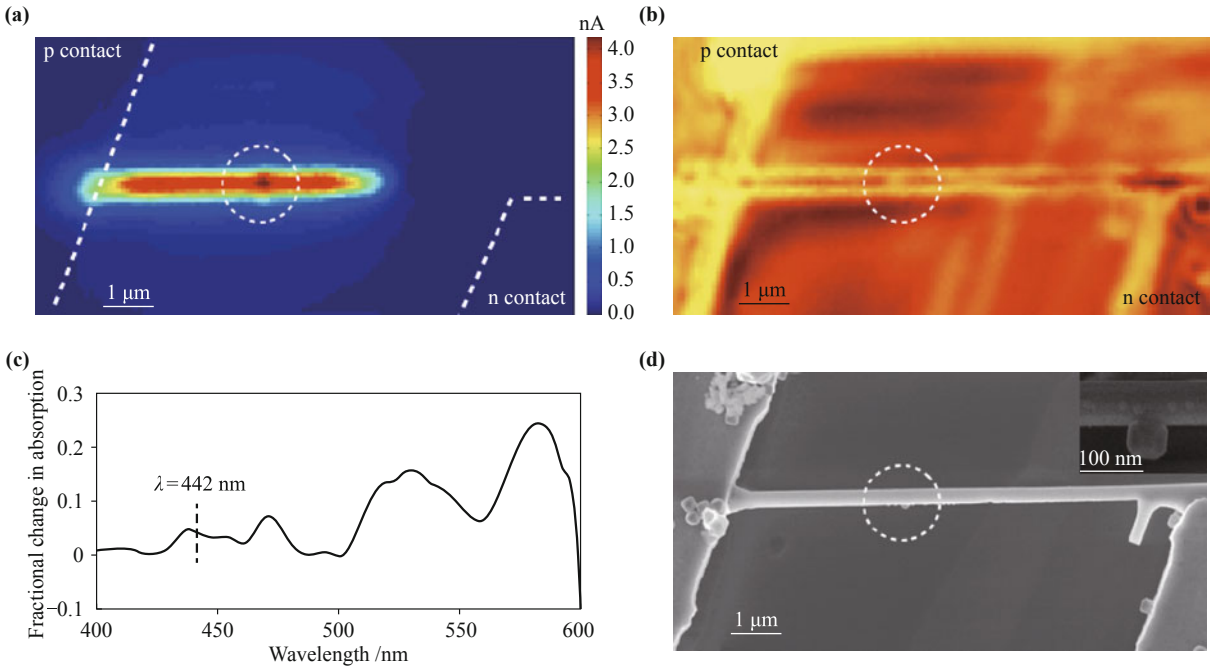

Fig. 5 **(a)** SPCM of a single-NW Si PV decorated with an octahedral silver nanocrystal. **(b)** Corresponding scanning optical image collected simultaneously showing scattering at the position of the nanocrystal. The scans were taken at a wavelength of $\lambda = 442$ nm. **(c)** The enhancement at the location of the nanoparticle is in agreement with a FDTD simulation for a NW this size. **(d)** SEM images of the device. Reproduced from Ref. [35], Copyright © 2011 American Chemical Society.

storage is a critical component to a renewable and sustainable energy future based on using sunlight as an energy source. Furthermore, a large component of our overall energy use is in the form of transportation fuels, which require a means to store the diffuse solar resource in a more concentrated resource. To address these issues, we have been investigating the direct conversion of solar energy into chemical fuels, through a process known as artificial photosynthesis [36–38]. In this process, we attempt to mimic what nature does every day in photosynthesis by storing the solar energy resource in the form of chemical bonds. The inputs to this process include sunlight, CO_2 and water, and the outputs could be in the form of gaseous or liquid fuels such as hydrogen, methanol, or longer-chain hydrocarbons. Besides storing solar energy for later use, this process attempts to close the cycle of CO_2 emissions associated with combustion reactions, resulting in a truly carbon-neutral process.

The implementation of artificial photosynthesis entails several strict requirements. In addition to the absorption and charge separation requirements of PVs, we must utilize excited charge carriers to drive electrochemical reactions in an efficient manner. This is typically done by forming a semiconductor-electrolyte interface, which allows for charge transfer reactions to occur driving the redox reactions in solution [39]. However, the kinetics of these reactions must occur at a high enough rate to extract the excited carriers before recombination occurs, which often time requires the inclusion of a co-catalyst material at the interface and loss of energy to electrochemical overpotentials. Furthermore, competing reactions such as corrosion or redox chemistry involving the semiconductor material can detrimentally affect the performance and lifetime of the devices. Therefore, we must seek robust and stable materials which can withstand the harsh conditions of PEC reactions in both a reducing and oxidizing environment.

While some semiconductor materials such as TiO_2 for solar water splitting have been shown to address many of these challenges [40], high efficiencies for single materials have been limited by insufficient absorption of the visible spectrum from high-bandgap metal oxide materials. To address this problem, researchers have shifted their focus to a PEC diode structure based on a coupled photocathode and anode material [41–43]. By splitting the overall reaction into two half-reactions at different interfaces,one can absorb a larger portion of the solar spectrum by a two-photon absorption process, which is similar to natural photosynthesis.

Semiconductor NWs possess several advantages for the implementation of artificial photosynthesis schemes [38]. Many of the favorable optical and electronic properties discussed in the NW PV section apply to photoelectrode materials, including improved light absorption, a minimized minority carrier diffusion length, and high-quality single crystalline materials. Additionally, the large surface areas associated with NW arrays can reduce activation overpotentials, by reducing the kinetic losses compared to planar devices. Therefore, we have focused our efforts on developing individual photocathode and anode materials, as well as developing strategies for integrating these materials into a dual-bandgap device capable of performing artificial photosynthesis. In the following sections, we will highlight recent examples of work on these individual components, and progress towards a fully integrated dual-electrode device.

3.1 NW photocathode materials

The photocathode is the location of the reduction half-reaction, where the fuel source is generated. The simplest photocathode reaction is the reduction of protons in water to produce hydrogen. This reaction involves the transfer of two electrons from the semiconductor to the electrolyte, producing one hydrogen molecule. Several candidate materials which have conduction band edges higher in energy than the H^+/H redox potential with suitable bandgaps for visible light absorption have been identified. Our research has focused on p-Si and p-GaP due to their favorable bandgaps and sufficient photovoltages to contribute substantially to the 1.23 V required for overall water splitting in a dual-bandgap device.

Silicon is a popular photocathode material due to its elemental abundance, favorable band alignment for the hydrogen evolution reaction, and the vast amount of knowledge in Si processing for PV materials [44, 45]. We have developed several methods for fabricating Si NW arrays, as highlighted in the NW PV section, based on both bottom-up and top-town processing. Due to relatively sluggish kinetics of hydrogen evolution, a co-catalyst is typically added to decrease the activation overpotential, which is typically Pt [39, 46] or MoS_x [47, 48]. These Si photocathodes have shown the ability to produce high photocurrent densities of over 20 mA/cm^2, which are required to achieve high conversion efficiencies in tandem devices. Our research is currently focused on reducing the cost of these materials through similar strategies as the Si NW PV array devices, by reducing material volume and purity requirements. Additionally, we are seeking to reduce the cost associated with the catalyst by searching for earth-abundant materials and seeking to reduce the Pt loading requirements by nanostructuring.

An alternate photocathode material of interest is GaP [41, 49], due to a conduction band edge of ∼1 V more negative than both the water reduction and CO_2 reduction potentials and relatively small bandgap (2.23

eV at 300 K). However, the majority of the GaP NW growth techniques reported have used high-temperature vapor phase approaches, which could add significantly to manufacturing costs of large-scale systems. Therefore, we developed a low-temperature solution-liquid-solid (SLS) growth process, which is capable of generating large scale quantities of NW product [50]. A key aspect of this process is that unlike previous SLS NW growth processes, the GaP NWs can be grown without the presence of surfactant molecules on the surfaces (Fig. 6). These surface species can hinder charge transfer reactions at the semiconductor-electrolyte interface, and are therefore not desirable for artificial photosynthesis.

The SLS process is similar to VLS NW growth, in which a metal catalyst particle becomes supersaturated with a reactant element, and a single-crystalline NW is precipitated which grows in a 1D manner. However, in this case, the reaction occurs in solution, allowing for a highly scalable reaction, which is not dependent on substrate surface area. Our GaP synthesis consists of injection of Ga and P precursors in a 1:1 molar ratio into a hot squalane solvent. The Ga precursor thermally decomposes to form nanoscale Ga metal droplets, which subsequently act as catalysts to promote the growth of GaP NWs. The resulting product consisted of GaP NWs with lengths of 1–2 μm, and diameters of ∼30 nm. Finally, the wires were cleaned and the Ga nanoparticles were selectively etched in an HCl solution, leaving the wires undamaged. A structural analysis by HRTEM and XRD confirmed that the wires were single-crystalline GaP, with visible light absorption measured by uv-vis spectrometry.

The PEC performance of the wires was measured by drop-casting a suspension of the wires in acetone onto a metal-coated glass substrate, followed by an inert gas anneal to make ohmic contact. The wires exhibited a positive increase in V_{oc} of ∼0.15 V under AM 1.5 1 sun illumination, indicating photocathodic behavior despite the fact that the wires were not intentionally doped. The ability to generate H_2 gas under visible-light illumination in neutral pH was measured using gas chromatography (GC) using methanol as a hole scavenger, and the H_2 evolution rate was increased by ∼1 order of magnitude when small Pt catalysts were loaded on the NW surface. Additionally, the stability of the wires under illumination in solution was confirmed by HRTEM images before and after a 18 h GC measurement, showing no noticeable difference in the NW surfaces.

In addition, we have developed a way to intentionally dope these wires with Zn by inserting diethylzinc (DEZ) into the reaction solution [51]. The Zn concentration in the wires could be controlled by varying the amount of DEZ injected into the solution. The p-type behavior of these wires was confirmed by single-NW field effect transistor (FET) measurements. The Zn-doping resulted in an increase in open-circuit photovoltage (up to 280 mV), and Mott–Shottky measurements gave a flatband potential of 0.52 V vs. RHE. An increase in carrier concentration due to the dopants results in an improved photovoltage and photocurrent compared to undoped wires, which is attributed to a reduced depletion region width to below the NW radius, preventing complete depletion of the NW. This is a central issue to both NW PV and PEC devices, indicating the importance of doping control in nanostructures.

An optimal doping concentration of 0.6%–1% Zn was found, leading to a photocurrent which is ∼80% that of planar GaP. Despite this lower value, the absorbed photocurrent efficiency (APCE) of the NW sample was consistently higher across visible wavelengths than the

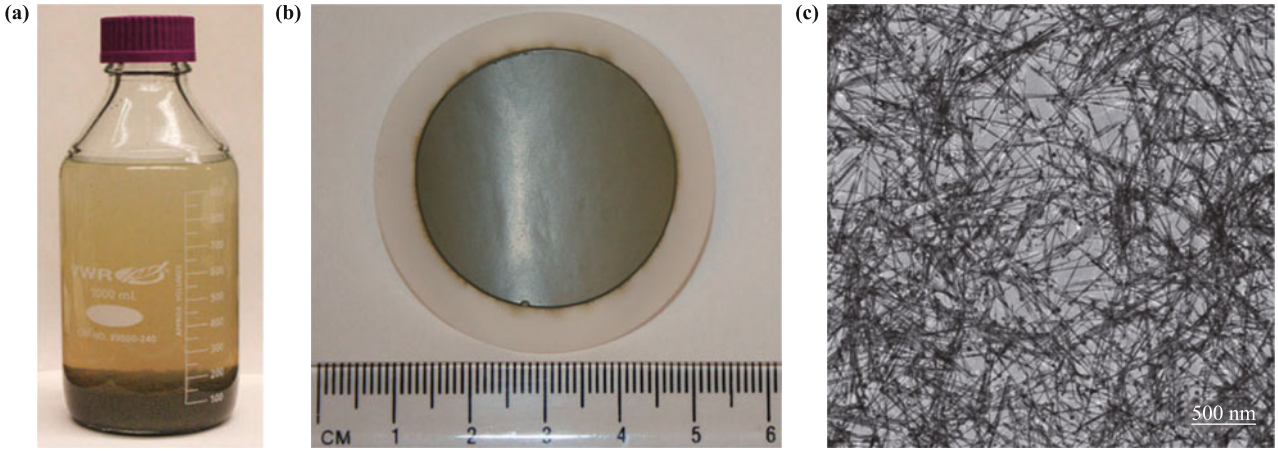

Fig. 6 Large-scale, solution synthesis of semiconductor nanowires. **(a)** As-synthesized GaP nanowires in 1 L of hexadecane. **(b)** A GaP nanowire membrane fabricated by filtration of water-dispersed GaP nanowires through a filter paper (white). After drying, the nanowire membrane became free-standing. **(c)** Transmission electron microscopy image of the GaP nanowires. Reproduced from Ref. [50], Copyright © 2011 American Chemical Society.

planar sample, showing improved charge separation efficiency. Furthermore, the APCE was shown to increase with decreasing loading of the NWs suggesting that charge transport across the NW/NW contacts limits the overall performance. Thus, with improved contact between the wires, the photocurrent could potentially be improved further. This study demonstrated the advantages of the NW geometry for PEC performance in GaP, by achieving comparable results while utilizing 1/3000 of the quantity of GaP in a planar wafer, with a higher APCE over the visible spectrum.

3.2 NW photoanode materials

The photoanode presents a more challenging set of requirements, due the photoanodic corrosion under of many semiconductor materials with appropriate band edges for the water oxidation reaction [39]. Therefore, metal oxide materials have been widely studied due to their stability under photoanodic conditions. However, due to the relatively low valence band edges of metal oxides compared to the water oxidation potential (+1.23 V vs. NHE), a significant loss in energy results due to the valence band offset. Furthermore, many metal oxide materials have large bandgaps, which limit the absorption of visible light, and therefore the overall photocurrent. Thus the search for an efficient photoanode material typically involves three approaches: increasing the visible light absorption of wide-gap metal oxides, thin surface coatings of unstable materials to improve stability against corrosion, and searching for new stable materials which absorb a greater portion of the visible spectrum.

Since the demonstration of water splitting using TiO_2 by Fujishima and Honda in 1972 [40], TiO_2 has been widely studied as a photoanode material due to its relative stability and low cost. However, due to the high bandgap of rutile TiO_2, as well as a low electron mobility and minority carrier diffusion length, the resulting photocurrents are too low for efficient implementation into a dual-bandgap tandem PEC device. NWs have the potential to improve the quantum efficiency of TiO_2 in the UV, by decoupling the absorption and diffusion lengths, as shown in Fig. 1. However, an increase in length also has certain disadvantages, such as increased surface recombination and difficulty in electron extraction due to a poor electron mobility.

To improve our understanding of these effects, we performed a study on rutile TiO_2 NW arrays to quantify the dependence of PEC performance on NW length and surface coatings [52]. Rutile TiO_2 NW arrays were grown on FTO substrates by a hydrothermal method, which allowed for control of NW length by varying the growth time. PEC measurements were performed on 4 different lengths of NW arrays, and an increase in the anodic photocurrent with increasing NW length from 0.28 to 1.28 μm was observed, which appeared to approach a saturation current. Furthermore, the IPCE spectra showed a red shift in the maximum EQE with increasing NW length. This suggests that carrier extraction can limit performance in longer wires for shorter wavelengths, which are absorbed near the top of the wires.

To further improve the energy conversion efficiency of TiO_2 NWs, a thin surface coating of TiO_2 was deposited on the NW arrays by ALD. This strategy has been used to improve charge collection efficiency by reducing surface states [53]. The ALD films were grown at 300°C using $TiCl_4$ and water as precursors. HRTEM and XRD analysis showed a variation in the phase of the ALD TiO_2 material from partially amorphous, to rutile, to anatase with increasing shell thickness. Interestingly, the rutile phase formed epitaxially on the NW core, as confirmed by HRTEM. The PEC performance of these coatings demonstrated a decrease in anodic photocurrent for the amorphous and anatase coatings, and an increase with the rutile coating. The increase in photocurrent for the rutile coating was attributed to a combination of increased surface passivation, increased surface area due to the polycrystalline shell, and an improvement of charge collection efficiency, as shown by an increase in the IPCE for shorter wavelengths.

Despite these improvements in TiO_2 NWs, the overall energy conversion efficiency of TiO_2 is limited by low absorption due to a high bandgap. Therefore, many groups are studying the ability to use TiO_2 or other stable oxide materials as surface coatings to protect otherwise unstable photoanode materials with smaller bandgaps [54]. This strategy requires the use of a thin and conformal coating layer, capable of oxidizing water at the interface between the coating layer and electrolyte, while preventing corrosion of the underlying light absorber under highly oxidizing conditions in solution. To demonstrate this effect, we deposited thin layers of TiO_2 on planar and NW Si substrates using ALD [55]. In this structure, UV-light is absorbed in the TiO_2, while visible light is absorbed in the Si. Holes generated in the TiO_2 oxidize water, while electrons generated in TiO_2 recombine with holes generated from the Si at the Si/TiO_2 interface. For both n-type and p-type Si, an increase in the saturation photocurrent of 2.5× that of planar substrates is observed in the NW samples, which is attributed to decreased reflectance and increased surface areas. Additionally, n-Si/n-TiO_2 samples exhibited higher photovoltages and photocurrents than p-Si/n-TiO_2 samples, due to favorable band-bending at the semiconductor heterojunction interface, which reduces losses from holes recombining at the heterojunction interface due to favor-

able band bending. Thus, while the oxidation photocurrent still comes from absorption in the shell material, the n-n junction can improve the short circuit current by decreasing recombination at the back surface of the shell, while providing a shift in V_{OC} towards more negative onset potentials.

While stabilizing lower-bandgap semiconductors by surface coating addresses the absorption and stability criteria separately, the ideal photoanode should have both of these qualities in one single material. Although several metal oxides have demonstrated stability against photoanodic corrosion, the valence band maximum is typically more than 1 eV below the redox potential for water oxidation. Therefore, much of the energy absorbed in oxide materials does not contribute to the useful energy extracted through water splitting. An alternate set of compounds is the metal nitride family, which has a higher valence band maximum due to the smaller ionization energy of N 2p orbitals compared to O 2p orbitals. In particular, $In_xGa_{1-x}N$ alloys have been shown to have a tunable bandgap from the UV to near-IR region of the spectrum [56]. This allows for tuning of the absorption properties to allow for a material capable of either overall water splitting, or acting as an efficient photoanode material.

We have previously developed a halide chemical vapor deposition (HCVD) technique for growing single-phase InGaN wires width tunable stoichiometries [56]. To study the PEC properties of these wires as a photoanode, $In_xGa_{1-x}N$ ($x = 0.08-0.1$) were grown on planar Si and Si NW array substrates (Fig. 7) [57]. The InGaN/Si hierarchical arrays provided a photocurrent at an onset voltage of 0.1 V vs. RHE, and reached a photocurrent density of 33 $\mu A/cm^2$ at 1.23 V vs. RHE. This was 5 times higher than the NW arrays grown on planar Si substrates, which attributed to a higher surface area for the electrochemical reaction and increased optical pathway in the hierarchical arrays. Furthermore, these NWs were stable against photoanodic corrosion or oxidation after 15h of continuous illumination in a pH=3 electrolyte at a high light intensity (350 mW/cm^2), as confirmed by HRTEM analysis.

Despite their promising onset voltage and stability, the photocurrent for these devices is only 1.2 % of the theoretical maximum based on their bandgap. This low current was attributed to fast recombination and sluggish charge transfer kinetics at the semiconductor interface. Efforts to improve the material quality and addition of a co-catalyst are potential areas of improvement for these structures. Therefore, the search for an efficient photoanode material continues, and is an important direction for future research.

3.3 Integrated dual-bandgap NW PEC systems

The final goal of the dual-bandgap PEC research is to generate a system capable of performing water splitting and artificial photosynthesis using only solar energy as an input. To achieve this goal, we need to develop architectures capable of integrating a photoanode and photocathode into a single, current matched device. To accomplish this difficult task, we have proposed two approaches: an asymmetric junction based on a core-shell structure with both materials present in a single NW, and a bilayer NW fabric.

As model system for demonstrating a two-bandgap scheme, we have developed the ability to fabricate a Si/TiO_2 asymmetric junction onto single NWs [58]. In this case, the Si acts as the photocathode where the reduction reaction occurs, and the TiO_2 acts as a photoanode to oxidize water. Asymmetric core-shell NW structures were fabricated by growing Si NWs via a VLS mechanism, which were subsequently coated by TiO_2 shell layers by ALD. These shells were removed from a part of the NW by masking and selective etching of the

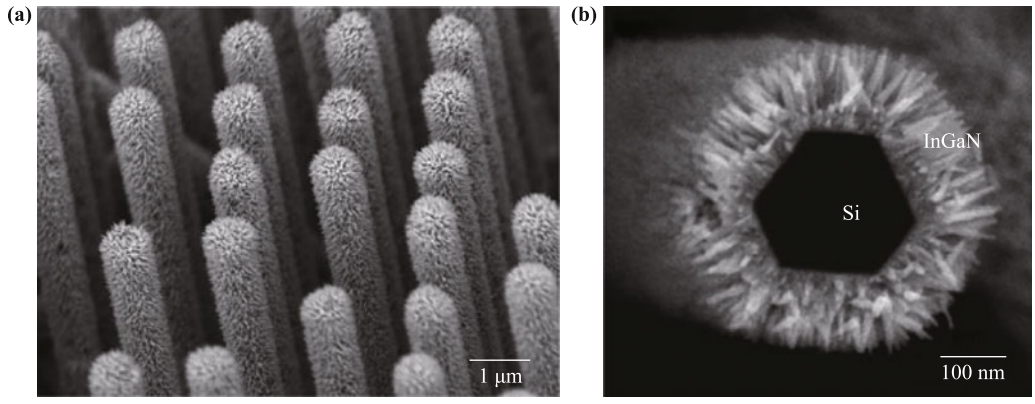

Fig. 7 High surface area Si/InGaN nanowire photoanodes. SEM images of hierarchical $Si/In_xGa_{1-x}N$ nanowire arrays on a Si (111) substrate with $x = 0.08$–0.1 **(a)**. A fractured wire reveals the cross-section **(b)** showing that InGaN nanowires grow vertically from the six Si wire facets. Reproduced from Ref. [57], Copyright © 2012 American Chemical Society.

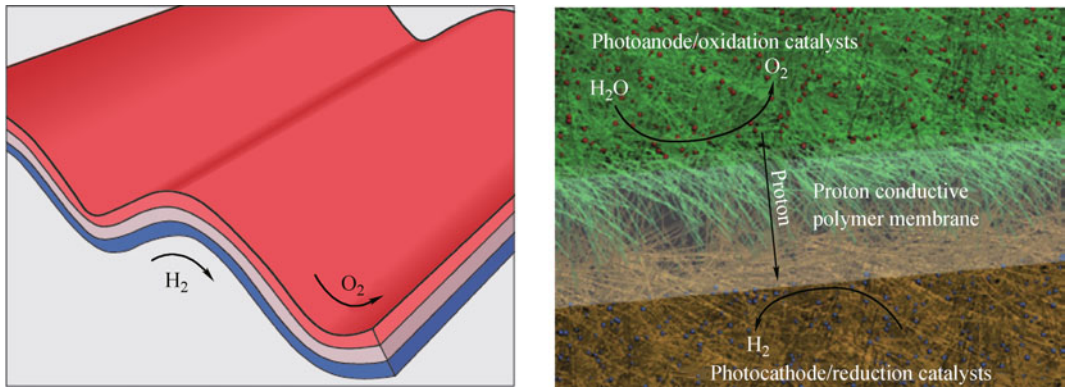

Fig. 8 Schematic illustration (left) and a zoomed-in view (right) of a bilayer nanowire fabric-based composite membrane for direct solar water-splitting. The top layer is a high-surface-area nanowire mesh decorated with oxidation catalysts. This part serves as a photoanode responsible for water oxidation; the bottom layer is a high-surface-area nanowire mesh decorated with reduction catalysts. This is the photocathode responsible for water reduction. Reproduced from Ref. [59], Copyright ©2012 Nature Publishing Group.

TiO_2, leaving an exposed Si surface.

A key necessity for the successful implementation of a dual-bandgap PEC system is the efficient recombination of majority carriers between the two materials, while the minority carriers drive the separate redox reactions at the anode and cathode. The asymmetric NW structure allows for a study of this charge separation phenomenon by probing a single NW. To demonstrate this effect, asymmetric Si/TiO_2 NWs were illuminated by UV light, and the surface potential was measured as a function of position on the NW using Kelvin probe microscopy (KPM). This is a scanning probe technique, in which a conductive atomic force microscope (AFM) tip is used to measure surface potential with nm resolution. Controlled humidity was used to condense water on the NW surface, leading to the formation of a semiconductor/electrolyte interface for both materials. An increase in the positive surface potential was measured in the TiO_2 region relative to the Si region upon illumination, which is attributed to a buildup of holes at the TiO_2 electrolyte interface, and electrons at the Si/electrolyte interface. This demonstrates the ability of asymmetric structures to separate minority carriers while allowing majority carriers to recombine at the interface.

While the asymmetric structure provides a model system for studying a dual-bandgap system at the single NW system, the fabrication of such structures requires expensive processing steps, and the separation of the product species will not be trivial. Therefore, we have begun to develop bilayer NW fabrics, based on solution processing and flexible, low-cost substrates [59]. The photoelectrode materials will consist of NW meshes with high surface area, using solution-processed NW materials such as our SLS grown NWs (Fig. 8). A proton conducting material will be placed between the electrode materials, and matching of the current densities will be required for efficient utilization of the solar resource. This will reduce the costs associated with high-temperature or vacuum processing, separation of product species, and the turnover frequency requirements of co-catalysts due to the use of high surface area electrodes. The major challenge now is to develop efficient photoanode materials, capable of generating sufficiently high current-densities to provide a large current in a current-matched dual-bandgap system.

4 Conclusion

Due to an improvement in light absorption, charge separation efficiency, high surface-areas for electrochemical reactions, and the ability to fabricate high-quality single-crystalline materials with high carrier mobility, semiconductor NWs are an attractive building block for solar photovoltaic and photoelectrochemical energy conversion. We have focused on a combination of developing large-scale NW arrays and single-NW devices to gain an improved understanding of the fundamental properties of these materials. In all cases, the end goal is to reduce the cost and improve the energy conversion efficiency, to enable large-scale adaptation of renewable energy. Through the use of less raw material, with lower purity and carrier lifetime requirements, combined with the favorable optical and electrical properties of NWs, hold great promise to enable a new generation of low-cost, high efficiency solar energy conversion devices.

Acknowledgements N. P. Dasgupta acknowledges support from the U.S. Department of Energy, Office of Energy Efficiency and Renewable Energy (EERE) Postdoctoral Research Awards under the SunShot Solar Energy Technologies Program. This work was supported by the Director, Office of Science, Office of Basic Energy Sciences, Materials Sciences and Engineering Division, of the U.S. Department of Energy under Contract No. DE-AC02-05CH11231.

References

1. E. C. Garnett, M. L. Brongersma, Y. Cui, and M. D. McGehee, Annu. Rev. Mater. Res., 2011, 41(1): 269
2. A. I. Hochbaum and P. Yang, Chem. Rev., 2010, 110(1): 527
3. B. M. Kayes, H. A. Atwater, and N. S. Lewis, J. Appl. Phys., 2005, 97(11): 114302
4. L. Hu and G. Chen, Nano Lett., 2007, 7(11): 3249
5. E. Garnett and P. Yang, Nano Lett., 2010, 10(3): 1082
6. N. P. Dasgupta, S. Xu, H. J. Jung, A. Iancu, R. Fasching, R. Sinclair, and F. B. Prinz, Adv. Funct. Mater., 2012, 22(17): 3650
7. O. L. Muskens, J. G. Rivas, R. E. Algra, E. P. A. M. Bakkers, and A. Lagendijk, Nano Lett., 2008, 8(9): 2638
8. L. Tsakalakos, J. Balch, J. Fronheiser, B. A. Korevaar, O. Sulima, and J. Rand, Appl. Phys. Lett., 2007, 91(23): 233117
9. M. A. Green, K. Emery, Y. Hishikawa, W. Warta, and E. D. Dunlop, Prog. Photovolt. Res. Appl., 2012, 20(5): 606
10. L. E. Greene, M. Law, D. H. Tan, M. Montano, J. Goldberger, G. Somorjai, and P. Yang, Nano Lett., 2005, 5(7): 1231
11. L. E. Greene, B. D. Yuhas, M. Law, D. Zitoun, and P. Yang, Inorg. Chem., 2006, 45(19): 7535
12. M. Law, L. E. Greene, J. C. Johnson, R. Saykally, and P. Yang, Nat. Mater., 2005, 4(6): 455
13. A. C. Fisher, L. M. Peter, E. A. Ponomarev, A. B. Walker, and K. G. U. Wijayantha, J. Phys. Chem. B, 2000, 104(5): 949
14. M. Law, L. E. Greene, A. Radenovic, T. Kuykendall, J. Liphardt, and P. Yang, J. Phys. Chem. B, 2006, 110(45): 22652
15. L. E. Greene, M. Law, B. D. Yuhas, and P. Yang, J. Phys. Chem. C, 2007, 111(50): 18451
16. B. D. Yuhas and P. D. Yang, J. Am. Chem. Soc., 2009, 131(10): 3756
17. M. D. Kelzenberg, S. W. Boettcher, J. A. Petykiewicz, D. B. Turner-Evans, M. C. Putnam, E. L. Warren, J. M. Spurgeon, R. M. Briggs, N. S. Lewis, and H. A. Atwater, Nat. Mater., 2010, 9(3): 239
18. J. Zhu, C. M. Hsu, Z. Yu, S. Fan, and Y. Cui, Nano Lett., 2010, 10(6): 1979
19. J. Zhu, Z. Yu, G. F. Burkhard, C. M. Hsu, S. T. Connor, Y. Xu, Q. Wang, M. McGehee, S. Fan, and Y. Cui, Nano Lett., 2009, 9(1): 279
20. E. Yablonovitch and G. D. Cody, IEEE Trans. Electron. Dev., 1982, 29(2): 300
21. M. G. Mauk, J. Miner. Met. Mater. Soc., 2003, 55(5): 38
22. A. Boukai, P. Haney, A. Katzenmeyer, G. M. Gallatin, A. A. Talin, and P. Yang, Chem. Phys. Lett., 2011, 501(4–6): 153
23. B. Tian, T. J. Kempa, and C. M. Lieber, Chem. Soc. Rev., 2009, 38(1): 16
24. M. D. Kelzenberg, D. B. Turner-Evans, B. M. Kayes, M. A. Filler, M. C. Putnam, N. S. Lewis, and H. A. Atwater, Nano Lett., 2008, 8(2): 710
25. B. Z. Tian, X. Zheng, T. J. Kempa, Y. Fang, N. Yu, G. Yu, J. Huang, and C. M. Lieber, Nature, 2007, 449(7164): 885
26. S. D. Oosterhout, M. M. Wienk, S. S. van Bavel, R. Thiedmann, L. Jan Anton Koster, J. Gilot, J. Loos, V. Schmidt, and R. A. J. Janssen, Nat. Mater., 2009, 8(10): 818
27. A. L. Briseno, T. W. Holcombe, A. I. Boukai, E. C. Garnett, S. W. Shelton, J. J. M. Fréchet, and P. Yang, Nano Lett., 2010, 10(1): 334
28. J. A. Czaban, D. A. Thompson, and R. R. Lapierre, Nano Lett., 2009, 9(1): 148
29. J. Tang, Z. Huo, S. Brittman, H. Gao, and P. Yang, Nat. Nanotechnol., 2011, 6(9): 568
30. L. Cao, P. Fan, A. P. Vasudev, J. S. White, Z. Yu, W. Cai, J. A. Schuller, S. Fan, and M. L. Brongersma, Nano Lett., 2010, 10(2): 439
31. L. Cao, J. S. White, J. S. Park, J. A. Schuller, B. M. Clemens, and M. L. Brongersma, Nat. Mater., 2009, 8(8): 643
32. V. E. Ferry, L. A. Sweatlock, D. Pacifici, and H. A. Atwater, Nano Lett., 2008, 8(12): 4391
33. K. Nakayama, K. Tanabe, and H. A. Atwater, Appl. Phys. Lett., 2008, 93(12): 121904
34. H. A. Atwater and A. Polman, Nat. Mater., 2010, 9(3): 205
35. S. Brittman, H. Gao, E. C. Garnett, and P. Yang, Nano Lett., 2011, 11(12): 5189
36. N. S. Lewis and D. G. Nocera, Proc. Natl. Acad. Sci. USA, 2006, 103(43): 15729
37. A. Listorti, J. Durrant, and J. Barber, Nat. Mater., 2009, 8(12): 929
38. P. Yang, MRS Bull., 2012, 37(9): 806
39. M. G. Walter, E. L. Warren, J. R. McKone, S. W. Boettcher, Q. Mi, E. A. Santori, and N. S. Lewis, Chem. Rev., 2010, 110(11): 6446
40. A. Fujishima and K. Honda, Nature, 1972, 238(5358): 37
41. A. J. Nozik, Appl. Phys. Lett., 1976, 29(3): 150
42. K. Ohashi, J. Mccann, and J. O. M. Bockris, Nature, 1977, 266(5603): 610
43. A. Kudo, MRS Bull., 2011, 36(1): 32
44. S. W. Boettcher, J. M. Spurgeon, M. C. Putnam, E. L. Warren, D. B. Turner-Evans, M. D. Kelzenberg, J. R. Maiolo, H. A. Atwater, and N. S. Lewis, Science, 2010, 327(5962): 185
45. S. W. Boettcher, E. L. Warren, M. C. Putnam, E. A. Santori, D. Turner-Evans, M. D. Kelzenberg, M. G. Walter, J. R. McKone, B. S. Brunschwig, H. A. Atwater, and N. S. Lewis, J. Am. Chem. Soc., 2011, 133(5): 1216
46. A. Heller, E. Aharon-Shalom, W. A. Bonner, and B. Miller, J. Am. Chem. Soc., 1982, 104(25): 6942
47. Y. Hou, B. L. Abrams, P. C. K. Vesborg, M. E. Björketun, K. Herbst, L. Bech, A. M. Setti, C. D. Damsgaard, T. Pedersen, O. Hansen, J. Rossmeisl, S. Dahl, J. K. Nørskov, and I. Chorkendorff, Nat. Mater., 2011, 10(6): 434

48. B. Hinnemann, P. G. Moses, J. Bonde, K. P. Jørgensen, J. H. Nielsen, S. Horch, I. Chorkendorff, and J. K. Nørskov, J. Am. Chem. Soc., 2005, 127(15): 5308
49. M. Tomkiewicz and J. M. Woodall, Science, 1977, 196(4293): 990
50. J. Sun, C. Liu, and P. Yang, J. Am. Chem. Soc., 2011, 133(48): 19306
51. C. Liu, J. Sun, J. Tang, and P. Yang, Nano Lett., 2012, 12(10): 5407
52. Y. J. Hwang, C. Hahn, B. Liu, and P. Yang, ACS Nano, 2012, 6(6): 5060
53. F. Le Formal, N. Tétreault, M. Cornuz, T. Moehl, M. Grätzel, and K. Sivula, Chem. Sci., 2011, 2(4): 737
54. Y. W. Chen, J. D. Prange, S. Dühnen, Y. Park, M. Gunji, C. E. D. Chidsey, and P. C. McIntyre, Nat. Mater., 2011, 10(7): 539
55. Y. J. Hwang, A. Boukai, and P. D. Yang, Nano Lett., 2009, 9(1): 410
56. T. Kuykendall, P. Ulrich, S. Aloni, and P. Yang, Nat. Mater., 2007, 6(12): 951
57. Y. J. Hwang, C. H. Wu, C. Hahn, H. E. Jeong, and P. Yang, Nano Lett., 2012, 12(3): 1678
58. C. Liu, Y. J. Hwang, H. E. Jeong, and P. Yang, Nano Lett., 2011, 11(9): 3755
59. P. Yang and J. M. Tarascon, Nat. Mater., 2012, 11(7): 560